Title

Limb bone scaling in hopping diprotodonts and quadrupedal artiodactyls

Authors

Michael Doube[1,2], Alessandro A Felder[2], Melissa Y Chua[1], Kalyani Lodhia[2], Michał M Kłosowski[1], John R Hutchinson[3], Sandra J Shefelbine[1,4]

Affiliations

1. Department of Bioengineering, Imperial College London, London SW7 2AZ, UK
2. Skeletal Biology Group, The Royal Veterinary College, Royal College Street, London NW1 0TU, UK
3. Structure and Motion Laboratory, The Royal Veterinary College, North Mymms, Hatfield, Hertfordshire AL9 7TA, UK
4. Department of Mechanical & Industrial Engineering, Northeastern University, 334 Snell Engineering Center, 360 Huntington Avenue, Boston, MA 02115, USA

Corresponding Author

Michael Doube

mdoube@rvc.ac.uk

Abstract

Bone adaptation is modulated by the timing, direction, rate, and magnitude of mechanical loads. To investigate whether frequent slow, or infrequent fast, gaits could dominate bone adaptation to load, we compared scaling of the limb bones from two mammalian herbivore clades that use radically different high-speed gaits, bipedal hopping and quadrupedal galloping. Forelimb and hindlimb bones were collected from 20 artiodactyl and 15 diprotodont species (body mass M 1.05 – 1536 kg) and scanned in clinical computed tomography or X-ray microtomography. Second moment of area (I_{max}) and bone length (l) were measured. Scaling relations ($y = ax^b$) were calculated for l vs M for each bone and for I_{max} vs M and I_{max} vs l for every 5% of length. I_{max} vs M scaling relationships were broadly similar between clades despite the diprotodont forelimb being nearly unloaded, and the hindlimb highly loaded, during bipedal hopping. I_{max} vs l and l vs M scaling were related to locomotor and behavioural specialisations. Low-intensity loads may be sufficient to maintain bone mass across a wide range of species. Occasional high-intensity gaits might not break through the load sensitivity saturation engendered by frequent low-intensity gaits.

Introduction

During daily rest and activity, bones experience a range of mechanical loading conditions that relate to each behaviour's physical intensity. Bones respond anabolically, that is, by increasing bone tissue formation and decreasing bone resorption, when they experience a small number of novel high strain and high strain rate events with a rest period between bouts of loading [1,2]. Repetitive loading has a saturation or habituation effect, in which tissue is no longer responsive to mechanical loads after a few tens of cycles [2]. Large numbers of loading cycles without sufficient rest are associated with fatigue or 'stress' fractures, typically seen in new military recruits [3] and racing animals such as greyhounds [4] and horses [5,6]. The distributions of occasional maximal loads and habitual moderate loads vary within the skeleton and depend on locomotor activity, which should appear as a morphological signal in clades that adopt very different characteristic gaits [7].

Kangaroos, wallabies and many of their diprotodont (including macropod) marsupial kin are famed for their hopping hindlimb gait which they use for bursts of efficient high-speed locomotion [8–10]. They are less well known for their slower pentapedal gait, wherein their powerful tail acts as the third point of a tripod with the forelimbs during hindlimb protraction [11] (Fig. 1). The pentapedal gait is used during grazing and other slow-speed activities, and dominates kangaroos' locomotor behaviour [10,12]. During hopping, the forelimbs are held away from ground contact for the entire stride cycle and thus are relatively unloaded [9], while hindlimb tissues experience near-ultimate stresses from ground reaction forces and muscle-tendon action, especially in larger diprotodonts [13]. The tail's role in pentapedal locomotion during slow-speed locomotion might enable reduced forelimb mass, potentially assisting more efficient bipedal hopping [11]. In extinct sthenurine macropods, the thoracic limb displays features of a browsing adaptation with elongated manus, reduced lateral digits, slender radius, ulna and humerus, and a 'human-like' scapula, which may have enabled these animals to forage browse above their heads [14]. Hopping is likely not possible at body mass over ~160 kg, at which the distal tendons' safety factor (ratio of actual to ultimate stress) drops below 1, meaning that extinct 'giant kangaroos' would have used slower gaits [13–16].

In contrast to diprotodonts, artiodactyl mammals (even-toed ungulates in the eutherian lineage; deer, sheep, camels and kin) have limited manual dexterity and quadrupedal gaits in

which the loads are spread more evenly among fore- and hindlimbs during slow and fast gaits, reflected in similarity of forelimb and hindlimb bones' cross-sectional properties [17]. Artiodactyls of several hundred kilograms, such as bison, buffalo, and giraffe, are capable of galloping [18,19], while hippopotami achieve high land speeds by a fast walk or trot [20]. Artiodactyls and diprotodonts spend a large proportion of their time grazing or resting as they are foregut fermenter herbivores [21] and may be considered ecological equivalents [22]. Scaling of limb bones in artiodactyls is relatively well characterised, exhibiting isometric or modestly allometric patterns [23–26]. Using artiodactyls as a baseline clade for comparison, here we ask investigate whether diprotodont limb bones exhibit structural scaling features that relate to their pentapedal and hopping locomotor specialisations.

If gaits involving high and rapidly applied strains were the main driver of bone shape scaling, then hindlimb bones should scale differently to forelimb bones in diprotodonts because the hindlimbs are loaded much more intensely than the forelimbs during hopping. Bennett (2000) pointed out that kangaroos' tibial cross-sections (section modulus Z and second moment of area I, which relate to fracture strength and resistance to bending respectively) scale more strongly than other quadrupeds [27], whereas McGowan et al. (2008) found that the macropod femur is more robust in larger animals lending support to the concept that intense hopping could relate to increased hindlimb robustness [28]. Positive allometry of hindlimb muscle physiological cross-sectional area, reduced duty factor with increasing speed, and constant effective mechanical advantage of hindlimb joints, together lead to relatively increased muscle force, and subsequently increased stress and reduced safety factors in larger macropods' hind limb bones and tendons, which may be partially ameliorated by increasing relative joint moments [16,28,29]. Musculotendinous forces generated during hopping could incur relatively larger loads on tendon insertion sites around the metaphyses compared to artiodactyls. Those larger loads in diprotodonts may manifest as stronger scaling of cross-sectional parameters in diprotodonts' metaphyses. Conversely, if the typical loading environment drives bone shape then we should expect to see similar scaling between diprotodonts' fore- and hindlimbs, and between equivalent bones in diprotodonts and artiodactyls, because the low speed pentapedal gait and quadrupedal walking respectively, dominate these clades' locomotor repertoires.

Using artiodactyls as a baseline clade, we ask whether diprotodont limb bones exhibit structural scaling features that relate to their pentapedal and hopping locomotor specialisations. In particular, we predict that the forelimb bones of the diprotodonts, which are used for grasping and low-speed locomotion (and are essentially unloaded during hopping), should have lower scaling exponents and become relatively more gracile with increases in body size than artiodactyl forelimbs and diprotodont hindlimbs. We hypothesise that scaling exponents should be more similar between fore- and hindlimb bones in artiodactyls than in diprotodonts due to artiodactyls' more even distribution of stresses between fore- and hindlimbs during high-speed locomotion.

Materials & Methods

We selected the humerus, radius, ulna, and metacarpal bone (III in diprotodonts and fused III-IV in artiodactyls), along with the femur, tibia and metatarsal bone (IV in diprotodonts and fused III-IV in artiodactyls) from 15 diprotodont and 20 artiodactyl species (Table 1). We imaged the bones in clinical computed tomographic (CT) scanners (LightSpeed 16, Ultra, or Pro 16, GE Medical Systems, Pollards Wood, UK) or for the smallest specimens, in an X-ray

microtomographic scanner (X-Tek HMX ST 225, Nikon Metrology, Tring, UK) with the bone's long axis positioned parallel to the image's *z*-axis, and applied a similar image processing technique used elsewhere [30,31]. Scans where the long axis of the bone was oblique to the *z*-axis of the scanner were aligned with BoneJ's Moments plugin, so that the bone's principal axes of inertia were parallel with the scan's x-, y-, and z-axes. Scans with large numbers of image slices were downsampled without interpolation to contain 100-200 slices. Fat in the marrow cavity and other bony or metal elements were manually replaced with a pixel value corresponding to air. Where nearby or fused bones could not be excluded by a rectangular region of interest (ROI), they were manually removed by replacing them with pixels of an air-equivalent value. Bones containing lesions or severe post-mortem deterioration were excluded from the study. Image analysis was performed with BoneJ v1.4.2 [32,33] for ImageJ v1.51c [34].

Second moment of area (I_{max}) was measured on every slice of each scanned specimen with Slice Geometry in BoneJ. Other parameters including I_{min}, cross-sectional area and section modulus were also measured and are available in the associated datasets [35], but are not reported here due to their close mathematical relationships: I is calculated by multiplying area by distance from the principal axis squared, and section modulus is calculated by dividing I by chord length. Because the ratios between specimen size, image resolution, and pixel spacing were not constant, we applied a correction for partial filling of pixels which maintains comparable cross-sectional area measurements when image resolution, pixel spacing and resolution vary with respect to each other (Figure 2). Partial filling correction was set by excluding pixels less than -800 HU to eliminate artefacts with values close to air (-1000 HU) and scaling linearly between -1000 HU (0% bone, 100% air) to 2300 HU (100% bone). Pixel values over 2300 HU were considered 100% bone. Images lacking HU calibration were set by taking a histogram of an ROI positioned in the background and using its mean for the 100% air scaling value and its maximum as the minimum cutoff value. Another histogram was made in a thick region of cortical bone and its mean used as the 100% bone scaling value. The partial volume correction approach was validated using synthetic images and an exemplar CT image, and resulted in a high degree of stability compared to global thresholding; test scripts and data are available online [35]. Bone length (l) was measured using the image data, which we validated against physical measurement of the bones. Body mass (M) was unknown for most of the specimens so was estimated from literature values [36–39]. The red and Eastern grey kangaroo specimens were male, so we used body masses near the high end of the estimate to account for the sexual dimorphism in these species.

We analysed scaling of bone dimensions using the general equation $y = ax^b$ [40], where y is the bone parameter, x is a measure of size (body mass M or bone length l), a relates to the scaling elevation and b is the scaling exponent. The exponent b expresses the rate of change in y as a function of body size, while a is the magnitude of y when $x = 1$. Scaling analysis relies on linear fitting to the log transformed variables, $\log(y) = \log(a) + b\log(x)$, where b becomes the slope of the line and $\log(a)$ the y intercept or 'elevation'. All scaling estimates were calculated using `smatr` version 3 [41] for R [42], using the standardised major axis (SMA, also known as RMA), which accounts for error in x as well as in y [43]. Cross-sectional parameters were averaged within each 5% increment of length and scaling exponents and elevations calculated for each 5% bin across all the individuals in each clade, for each bone in the study. Normalized cross-sectional parameters were calculated by dividing the nth root of the parameter by length. Second moment of area has units of mm^4, so it was normalized by

taking the 4th root and dividing by bone length in mm. Normalized parameters are unitless and a size-independent measure of shape.

To control for non-independence of samples due to their phylogeny, phylogenetically independent contrasts (PIC, [44]) were calculated for bone length, and I_{max} at mid-shaft (50% of bone length), using custom scripts that call functions from the `ape` and `smatr` R packages [35]. The calibrated phylogenetic trees used for PIC were constructed based on divergence time estimates from a previous publication; values from the two Eastern grey kangaroo specimens were averaged for PIC analysis ([45]; Figure 3).

Results

Bone length versus body mass comparisons (Table 2, Figure 4) indicate that artiodactyl metacarpal bones are much longer than in diprotodonts of similar mass, indicated by the high elevation (1.47 vs. 0.86). Humerus, radius and ulna lengths scale with positive allometry ($b > 0.33$) in diprotodonts, but with isometry (b not significantly different from 1/3) in artiodactyls. In the hindlimb, femur and metatarsal lengths scale similarly in diprotodonts and artiodactyls, with the diprotodont femur having a higher elevation than artiodactyls and the metatarsals' slopes and elevations not significantly different. Tibia length scales isometrically in artiodactyls and with strong positive allometry in diprotodonts. Comparing stylopod (humerus, femur), zeugopod (radius, ulna, tibia), and autopod (metacarpal, metatarsal) elements between limbs within each of the two clades, there is a high degree of overlap between the confidence limits of scaling exponents in all the limb segments, meaning that bone length proportionality between fore- and hindlimb segments is maintained within clades.

Normalized I_{max} versus per cent length plots (Figure 5) reveal that artiodactyls' cross-sections become relatively more robust with increasing body mass, indicated by the larger animals' traces tending towards the top of the range. Meanwhile, diprotodonts show the opposite trend, with normalized I_{max} decreasing with increasing body mass so that traces from the larger animals appear at the bottom of the range, indicating increased gracility with increasing body mass. In general, and in common with prior studies on cats and birds [30,31], the diaphysis occupies a decreasing proportion of bone length with increasing body mass. Notably, the trochlear notch and coronoid processes of the ulna drift distally in larger artiodactyls, but proximally in larger diprotodonts (Figure 5e, f).

Scaling exponents (Figure 6) and elevations (Figure 7) for I_{max} versus M reveal near-identical scaling exponents between clades for all regions of all the bones, and overlapping elevations for all bones in all regions except for the proximal tibial and femoral metaphyses, indicating very similar bone cross-sectional scaling against body mass. Positive allometry (exponent above the isometry line) is strongest in the proximal metaphyses, and this is amplified by increased elevations (i.e. larger value of I_{max} at a given M) in these regions in diprotodonts (Fig 7f, l, n). I_{max} versus l scaling reveals positive allometry for much of the length of artiodactyl bones. The wide confidence interval of artiodactyl ulna (Figure 6e) likely reflects the variability of fusion to the radius, reducing the strength of the body size signal. In contrast, diprotodont I_{max} scales with negative allometry against l for much of the length of humerus, radius, ulna and tibia, with positive allometry in the femur and isometry in the metacarpal and metatarsal. The raised elevation of diprotodonts relative to artiodactyls in the I_{max} versus l plots (Figure 7) is difficult to interpret because the scaling exponents are markedly different between clades in the regions where elevations are different. Despite their orders of

magnitude difference the elevations may not relate to functional differences, which may be more strongly indicated by differing scaling exponents.

Scaling exponents for diprotodont bone length and mid-shaft I_{max} corrected for phylogenetic effects using PIC were in general slightly higher, but remained within the 95% confidence interval of the scaling exponents calculated without phylogenetic correction (Table 3). PIC preserved statistically significant relationships (p=0.005) for diprotodont bone lengths with slightly lower squared correlation coefficients (non-PIC R^2 in [0.80,0.97], PIC R^2 in [0.55,0.95]). PIC analysis suggested that diprotodont femur and third metacarpal lengths scale isometrically, while all other diprotodont bone lengths scale with positive allometry. Diprotodont mid-shaft I_{max} does not scale differently from isometry (p: humerus 0.12; radius 0.33; ulna 0.09; metacarpal 0.38; femur 0.04; tibia 0.09; metatarsal 0.02) according to our PIC analysis.

Independent contrasts of artiodactyl bone lengths scale isometrically (slope not different from 0.33, p: humerus 0.48; radius 0.11; ulna 0.25; metacarpal 0.04; femur 0.08; tibia 0.92; metatarsal 0.17). Mid-shaft I_{max} tends to scale with positive allometry, and the significance of this relationship is strengthened by correcting for phylogeny. Artiodactyl bone length and mid-shaft I_{max} exponents calculated with PIC were higher than their uncorrected counterparts, remaining mostly within the uncorrected confidence intervals. Although their PIC-corrected and uncorrected confidence intervals overlapped, some PIC-corrected scaling exponent estimates (for femoral and tibial lengths, and femoral, tibial and metatarsal I_{max}) were outside the uncorrected confidence interval and vice versa. R^2 for artiodactyl bone lengths was again slightly decreased for PIC ([0.8,0.97] for uncorrected vs. [0.71,0.95] for PIC), but the relationships were significant in both PIC-corrected and uncorrected cases ($p<0.001$). In summary, scaling exponents calculated using PIC for bone length, mid-shaft CSA and mid-shaft I_{max} generally confirm the uncorrected scaling relationships. This result suggests that phylogeny has a minor influence on the scaling of bone geometry scaling within the two clades of mammals studied here.

Discussion

Scaling of the forelimb and hind limb segments is similar within clades, except the stylopod, in which the I_{max} versus length scaling displays positive allometry in the artiodactyl and diprotodont femur and artiodactyl humerus, but negative allometry in the diprotodont humerus, meaning that in diprotodonts the humerus becomes more gracile with increasing length while the femur becomes more robust. Unlike Bennett (2000), who found that tibial second moment of area scales more strongly positively in kangaroos than quadrupeds (b = 1.52 *vs* 1.28) [27], our data show that tibial cross-sections scale similarly against body mass between clades. This may be a consequence of comparing diprotodonts to artiodactyls only, and not to a more diverse sample of quadrupeds, because it is known that artiodactyls' bones scale differently to other mammalian clades [25,26]. Tibial cross-sections scale strongly negatively allometrically in diprotodonts and positively allometrically in artiodactyls against length. This means larger kangaroos' tibiae are relatively less robust – they are relatively longer and more slender consistent with a relatively reduced ability to resist bending moments. This apparent reduction in relative bending strength is surprising considering that bending stresses predominate over compressive stresses due to the off-axis component of the muscular forces, with a stress range of -110 to -60 MPa and 90-110MPa [8]. The I_{max} versus body mass scaling elevation is higher in the diprotodont proximal femur and tibia than the

same region in the artiodactyl femur and tibia, indicating increased robustness around the greater and lesser trochanters and tibial crest, which are the bony insertions for the massive gluteal, iliopsoas, and quadriceps muscle groups that drive bipedal hopping in diprotodonts. Positive allometry of tarsal joint moment arms potentially ameliorates the musculotendinous compressive force on the tibia during tarsus extension [28], allowing the distal half of diprotodonts' tibial cross-sections to remain within similar parameters as artiodactyls'. Like McGowan et al. (2008) demonstrated in macropods, we find that the femur is more robust in larger diprotodonts [28], which is consistent with a proposal of a universal relation between stylopod cross-sectional parameters and body mass [7]. We find that humeral and femoral lengths scale significantly differently against body mass between diprotodonts and artiodactyls, in contrast to suggestions of common mammalian femur length to body mass scaling [46], which may have implications for midshaft bending stresses.

The largest extant artiodactyls are an order of magnitude more massive than the largest extant diprotodonts while the smallest of both clades included in this study are ~1-2 kg. It would be unwise to extrapolate diprotodont scaling trends beyond the current series, because bipedal hopping was likely not a feature of the extinct giant kangaroos and may not be physiologically possible beyond ~160 kg [13–16]. Janis et al. (2014) suggested that large, extant kangaroos are functionally specialised for hopping in contrast to their larger extinct kin that did not hop, somewhat similar to the medium-sized, gracile and hyper-athletic cheetah (*Acinonyx jubatus,* M = 35-70 kg) compared to bigger and more robust felids such as lion (*Panthera leo*, M = 120-250 kg) [15].

We found that the trochlear notch of the ulna is relatively more distal in larger artiodactyls, but that an opposite trend of a relatively shortened olecranon process and proximally drifting trochlear notch is observed with increasing mass in diprotodonts. We first noticed a trend to a more centrally-placed trochlear notch in the ulna of large felids [30], and proposed that this may be a mechanism that may allow reduced muscle forces by increasing the lever arm of the olecranon process and increasing the elbow extensor muscles' effective mechanical advantage. The relatively shortening olecranon in larger diprotodonts may relate to forelimb use in the low-intensity pentapedal gait and lack of loading in high-intensity bipedal hopping, or to reaching and combat behaviours favouring a longer forelimb. Inter-clade differences in metacarpal dimensions relate to their functional specialisations for grasping, or plantigrade or unguligrade locomotion in diprotodonts and artiodactyls respectively. Similar isometric I_{max} scaling exponents against length indicate maintenance of overall bone shape that may relate to specialised manus function, whereas positive allometry against body mass in artiodactyls but isometry in diprotodonts may reflect an influence of locomotor loading on artiodactyl metacarpal robustness that is absent or reduced in diprotodonts.

Bone's mechanobiological response saturates after small number of load cycles [2], and variable safety factors among species and bones [47–49] suggest that peak strains from uncommon or high energy gaits are not necessarily the dominant stimuli for bone adaptation. Changes to habitual behaviour without a change in intensity (such as turning more often) can result in altered diaphyseal geometry [50], and habitual high unilateral loads, such as 12 hours per week of baseball throwing practice, lead to substantial cortical bone adaptation in the exercised limb [51]. The mouse tibia receives < 300 με (microstrain) during walking and < 600 με after a 30cm jump (~ 3N physiological load), yet requires at least 1000 με from a 10N experimental load to stimulate further bone formation [52–54]. Sciatic neurectomy removes

daily habitual loading in the mouse hindlimb, sensitising the tibia to subsequent load-induced (2000 με) bone deposition [55], suggesting that the removal of background stimulus can rescue bone's load responsiveness [56], or in other words, that daily stimulus saturates bone's ability to respond to further applied loads. In Thoroughbred horses, medium intensity training superimposed on spontaneous paddock exercise resulted in little increase in diaphyseal cross-sectional area [57] and rapid closing of secondary osteons in the metatarsal and metacarpal bones, whereas high intensity training resulted in ~10% increase in cortical area [58].

The lack of a difference in femoral and tibial I_{max} versus body mass scaling exponents between bipedal hopping diprotodonts and quadrupedal artiodactyls suggests that the occasional very high load of hopping may not be sufficient to overcome the mechanobiological saturation engendered by frequent but lower intensity loading in crouching and pentapedal walking. Alternatively, bipedal hopping may be a no more intense stimulus to the hindlimb than quadrupedal galloping, leading to little discernible difference between clades. However, we found similar $I_{max} \sim M$ scaling exponents in the forelimb bones, despite diprotodonts' relatively unloaded forelimbs during bipedal hopping. Simple body mass support and the ground reaction forces incurred by a slow gait may be sufficient to maintain cross-sectional bone geometry, while infrequent high intensity quadrupedal gaits might offer little further stimulus to diaphyseal size over and above that provided by standing and walking.

There are few data on the daily numbers of stride cycles in each gait for the species in the study, which limits our ability to calculate bone loading histories and infer which gaits relate most strongly to bone structural scaling, however, in those species that have been studied low intensity behaviours predominate. In large diprotodonts, the most frequent behaviour is lying down or standing still, followed by slow locomotion and only very occasional hopping [10,12]. In their highest activity periods in the 10h around dawn and dusk, tammar wallabies (*Macropus eugenii*) spend ~6% of their time in pentapedal walking, and only 3-5% (18-30 min/10h) of their time in bipedal hopping. The most frequent daylight posture is bipedal standing (50-70%) followed by quadrupedal crouching (15-30%), bipedal rearing (3-12%), and lying down (0-6%) [59]. Locomotion comprises only 5-10% of the behavioural repertoire of the parma wallaby (*Macropus parma*) [60]. Red and grey kangaroos (*Macropus rufus* and *M. giganteus*) spend the day alternating between lying, standing, crouching, grazing, and licking [12]. Agile wallabies' (*Macropus agilis*) most common behaviour is foraging (73%), followed by 'vigilance' (23%), and locomotion (0-6%) [61]. In grey kangaroos, over 90% of daily activity is crouching and lying, with only 0.0-3.3% accounted for by 'moving' [62]. Artiodactyls are similarly slow most of the time: wildebeest (*Connochaetes* sp.) travel only 2-3km daily [63]; red deer (*Cervus elaphus*) move on average 100-400m per hour [64], while giraffe walk for 5h daily [65] and can canter for only a few minutes at a time [66].

A scaling trend in gait preference might exist, such that small animals hop, trot or gallop more frequently than large animals, which could influence the interpretation of our results. Galloping and hopping engender similar muscle stresses at preferred speeds in rats and kangaroo rats respectively despite a fourfold difference in ground reaction force [67]. Diprotodont species that live in open country generally have a shorter period of suspension than those that live in dense forests or rocky hills, with a potential phylogenetic contribution to duty factor [9] and thus peak ground reaction forces and bone strains. Our PIC analysis found only limited effects of phylogeny on skeletal scaling parameters, suggesting little relationship between behavioural ecology, locomotor style, and bone geometry scaling within

diprotodont and artiodactyl clades. Comprehensive behavioural ecology, activity pattern, kinematic, ground reaction force, and tissue strain data would help to place the anatomical scaling that we have identified into the context of functional loading. Kinematic data exist for sheep, goats [68,69], pigs [70], cattle and a small number of other artiodactyls during walking [71] and for a small number of diprotodonts [72–74], but bone strain data are missing in all but a few species [69,75].

The lack of differential cross-sectional scaling in the diprotodont hindlimb despite their hopping behaviour led us to the speculation that their bones might have enhanced fatigue damage repair by increased remodelling, thus reducing the need for extra bone mass. We failed to find secondary osteonal remodelling in a *Macropus giganteus* femur sample, which was somewhat unusual for an animal of 33kg body mass [76]. Absence of secondary osteons may relate to the single sample failing to include any by chance, or a load-related suppression of remodelling protecting bone from local weakening due to osteoclastic resorption [58]. The current and other studies of bone organ allometry assume no size-related variation in bone microstructure or physiology and that all mammalian bone has similar biomechanical and mechanobiological behavior. Our recent work demonstrated that secondary osteons are wider in larger animals and narrower in smaller animals [76], and that trabeculae are thicker and more widely spaced in larger animals [77] indicating that biophysical constraints or cellular behaviour may vary among mammals and potentially interact with organ-level scaling. Integration of macro- and micro-level perspectives in future scaling studies could be particularly informative.

Forelimb-hindlimb and bipedal-quadrupedal comparisons of scaling relationships have revealed very similar cross-sectional scaling against mass in the primary weightbearing limb bones in artiodactyls and diprotodonts, despite differences in their high intensity gaits, suggesting that habitual low loads rather than occasional high loads may be the dominant stimuli for bone modelling. Cross-sectional scaling against length meanwhile appears to relate to clade-related specialisations such as diprotodonts' long, gracile forelimb used in low-speed weightbearing and grasping food, and artiodactyls' more robust forelimb bones specialised for cursorial locomotion.

Data Accessibility

Code, scripts, and databases [35] and raw and processed images [78] are available on figshare under a CC-BY licence. BoneJ is available from bonej.org and v1.4.2 source code is at zenodo [33].

Competing interests

The authors declare that we have no competing interests

Authors' contributions

MD collected and imaged specimens, wrote code, analysed the data, and drafted the manuscript; AAF performed the phylogenetic independent contrasts and helped to draft the manuscript; MMK performed X-ray microtomography; MYC and KL performed preliminary analyses; SJS and JRH conceived of and designed the study, and helped draft the manuscript. All authors gave final approval for publication.

Acknowledgements

For help with specimen loans we thank Matt Lowe at the University Museum of Zoology, Cambridge, and Roberto Portela-Miguez and Louise Tomsett at the Natural History Museum London. Richard Abel assisted with X-ray microtomography, Renate Weller and Charlotte Mumby assisted with computed tomography, Andrew Cuff advised on phylogenetic independent contrasts and Alexis Wiktorowicz-Conroy gave valuable advice regarding diprotodont gait. We thank Andrew Pitsillides and Behzad Javaheri for helpful conversations about bone mechanobiology.

Funding statement

This work was supported by UK Biological and Bioscience Research Council grants to SJS (BB/F001169/1) and JRH (BB/F000863/1). AF was supported by an RVC PhD studentship.

Figures

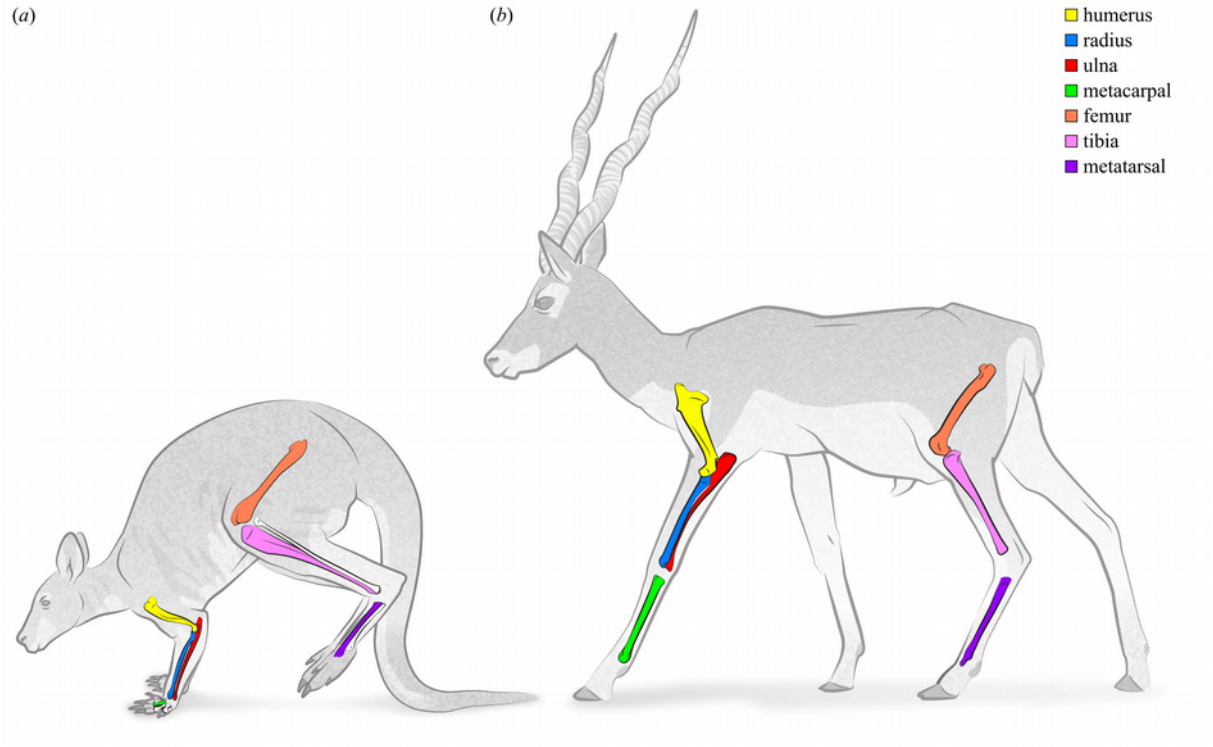

Figure 1. Bennett's wallaby (*Macropus rufogriseus*) in the hindlimb suspension phase of the pentapedal gait (a) and blackbuck (*Antelope cervicapra*) in a lateral sequence walk (b) indicating the limb bones measured in the study. These two species have femora of similar length (199 mm and 186 mm respectively) and are presented here approximately to scale. Drawing by Manuela Bertoni may be reused under the CC BY licence.

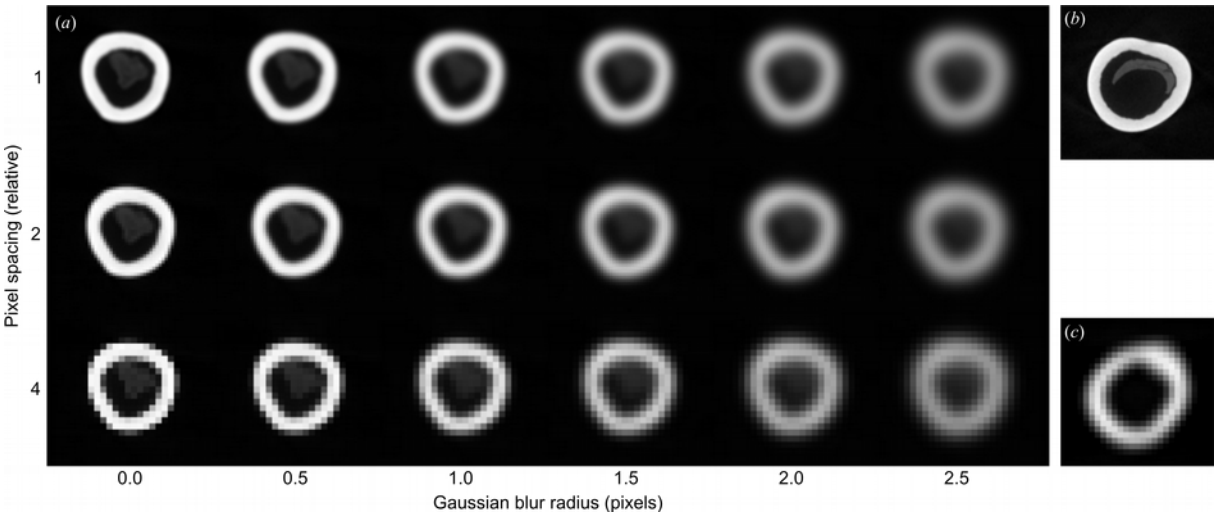

Figure 2. Interaction between specimen size, image resolution and pixel spacing. As pixel spacing increases and resolution decreases relative to specimen size, a greater proportion of pixels represent the edge of the specimens compared to the mid-substance. (a) Progressive downsampling of a well-sampled image of a bone cross-section (top left) increases pixel spacing (vertical axis) and Gaussian blurring with increasing radius simulates lower instrument resolution (horizontal axis). High-resolution images from X-ray microtomography (b) and lower resolution clinical CT images (c) relate to different pixel spacing/image resolution combinations within this scheme. We corrected for imaging condition and specimen size variation using a weighted pixel sum approach in BoneJ's Slice Geometry plugin.

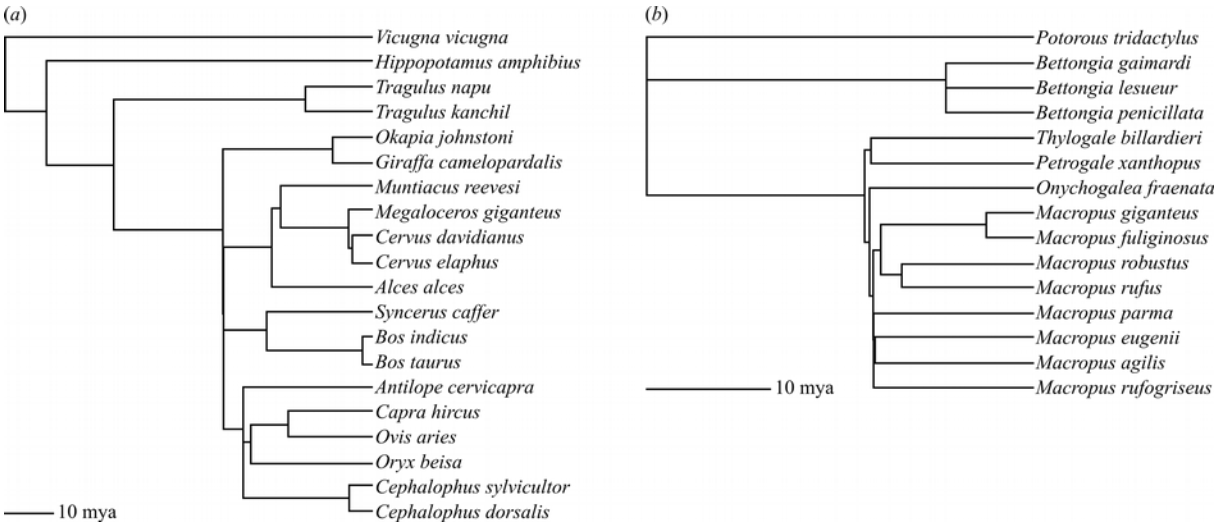

440 **Figure 3**. Cladograms illustrating phylogenetic relationships (from [45]) among the artiodactyl (a) and diprotodont (b) species used to perform phylogenetic independent contrast calculations.

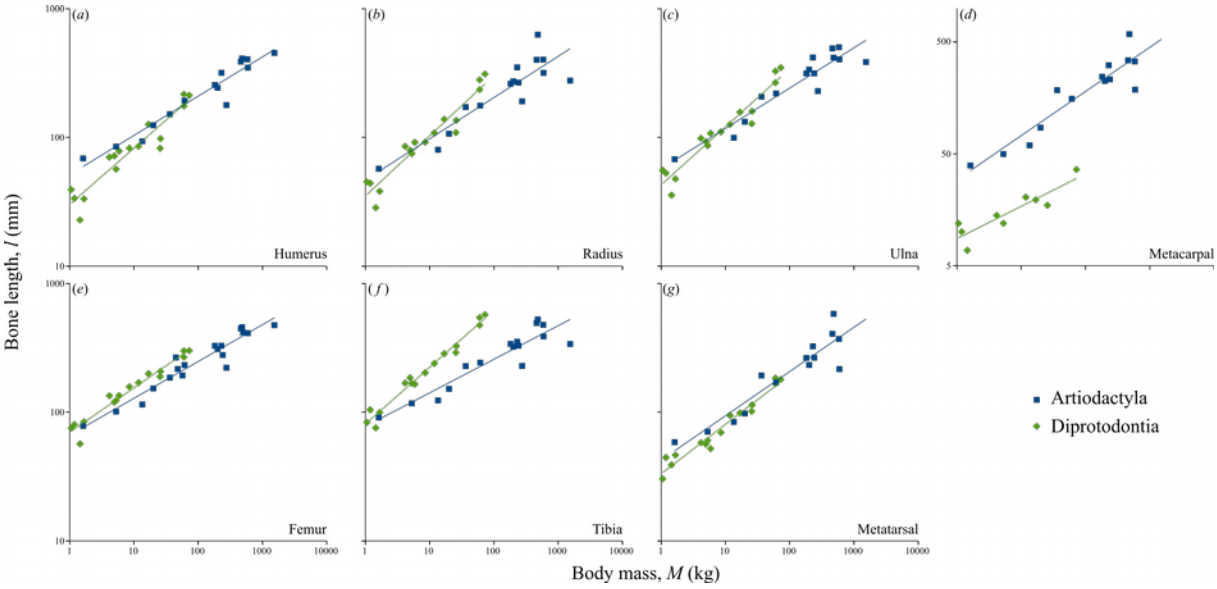

Figure 4. Bone length (l) versus body mass (M) regressions for all bones. Scaling exponents (slopes, b), elevations ($\log_{10}(a)$), R^2 and p values are presented in Table 2.

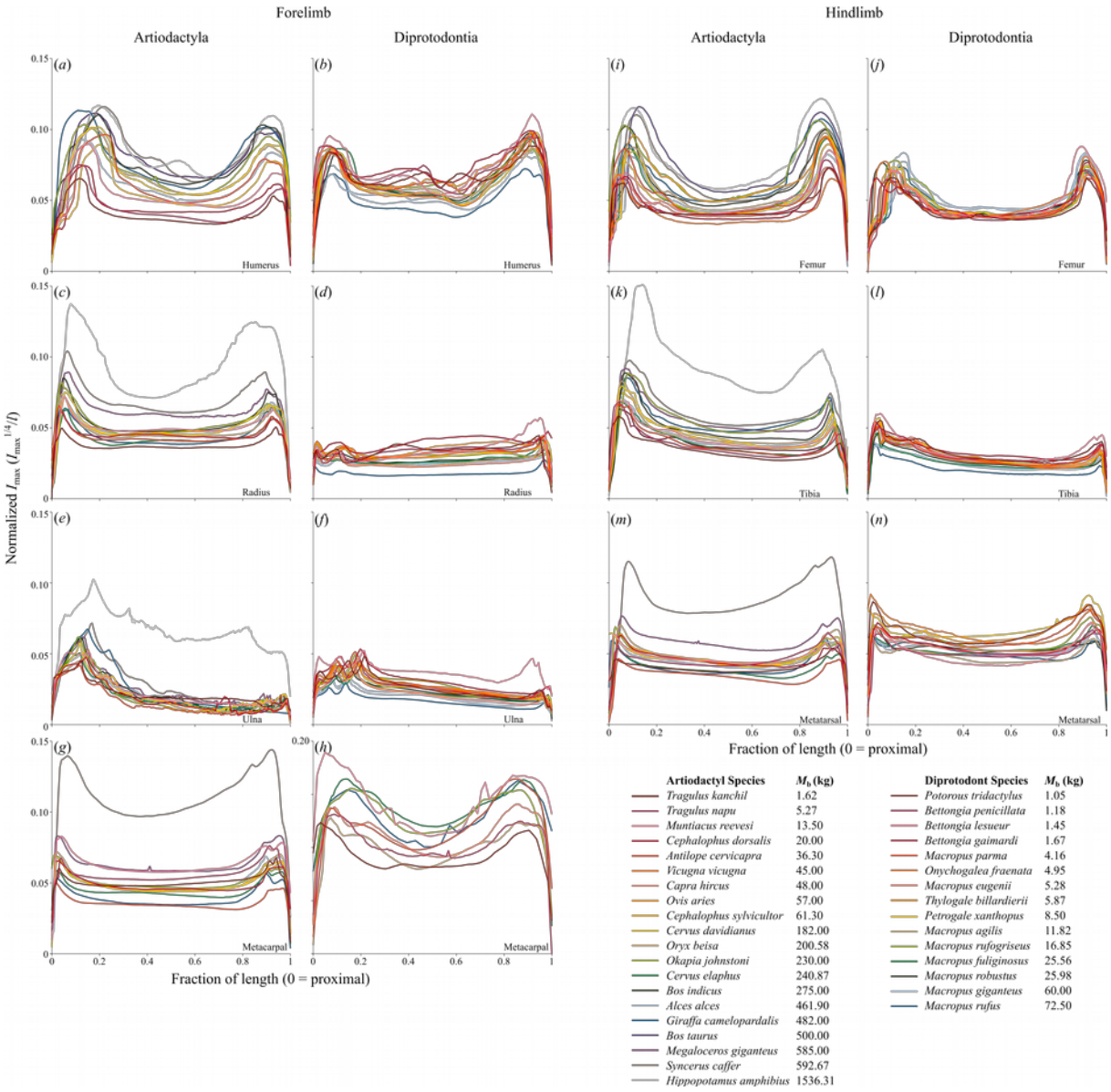

Figure 5. Normalized second moment of area ($I_{max}^{1/4}/l$) at each fraction of length. Dispersal of traces indicates bone shape differences among species. Higher traces indicate relatively more robust bone geometry, seen in larger artiodactyls and smaller diprotodonts. Note the increasing proportion of length occupied by epiphyseal and metaphyseal components in larger artiodactyl species (*a*, *i*), and the distal drift of the ulna's trochlear notch in larger artiodactyls (*e*) and smaller diprotodonts (*f*).

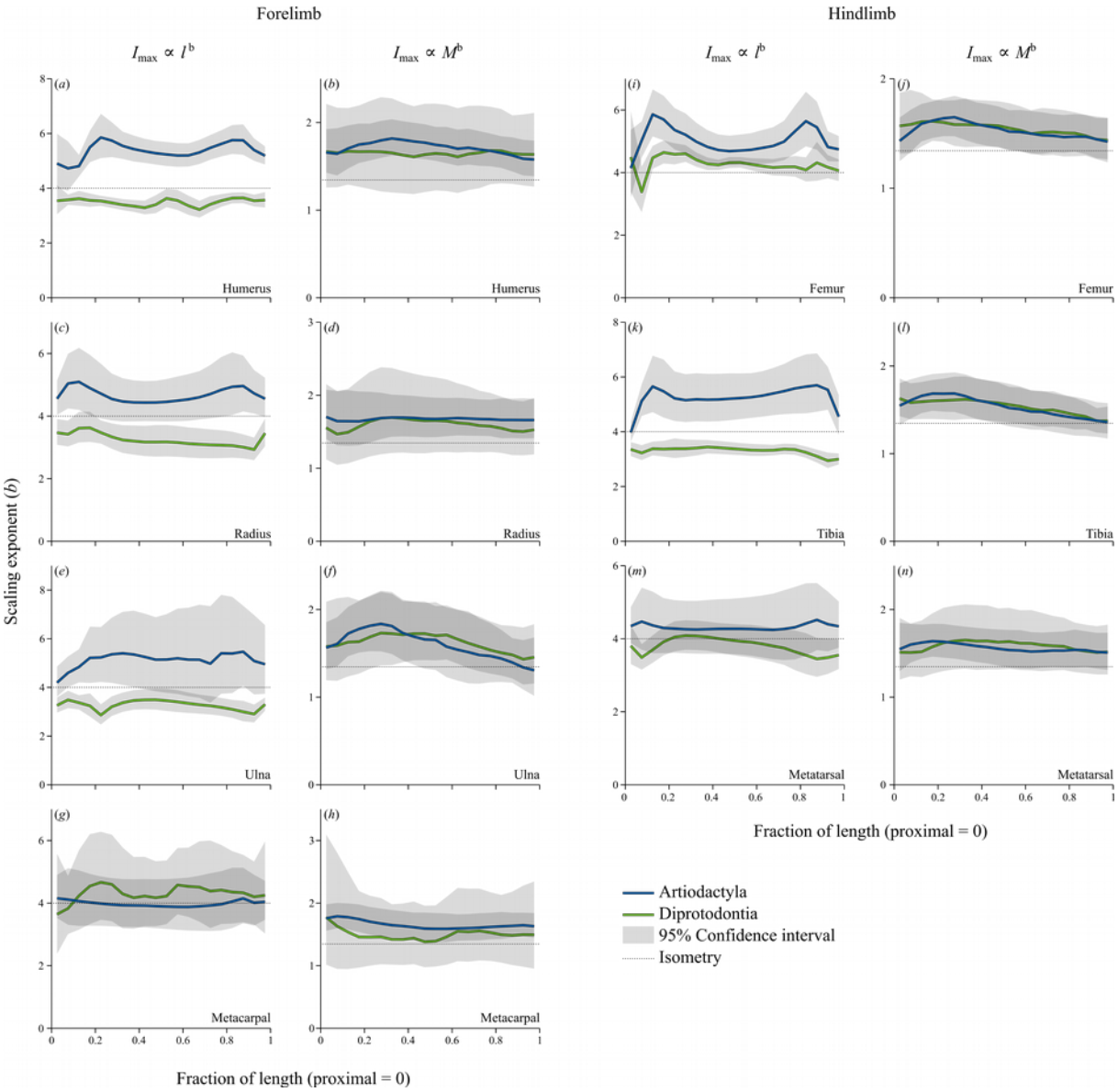

Figure 6. Scaling exponents for second moment of area (I_{max}) versus bone length (l) and body mass (M) for all bones and both clades. Light grey regions indicate the 95% confidence interval; dark grey regions occur where the confidence intervals overlap and may be interpreted as no significant difference in scaling exponent in that region of the bone, between clades.

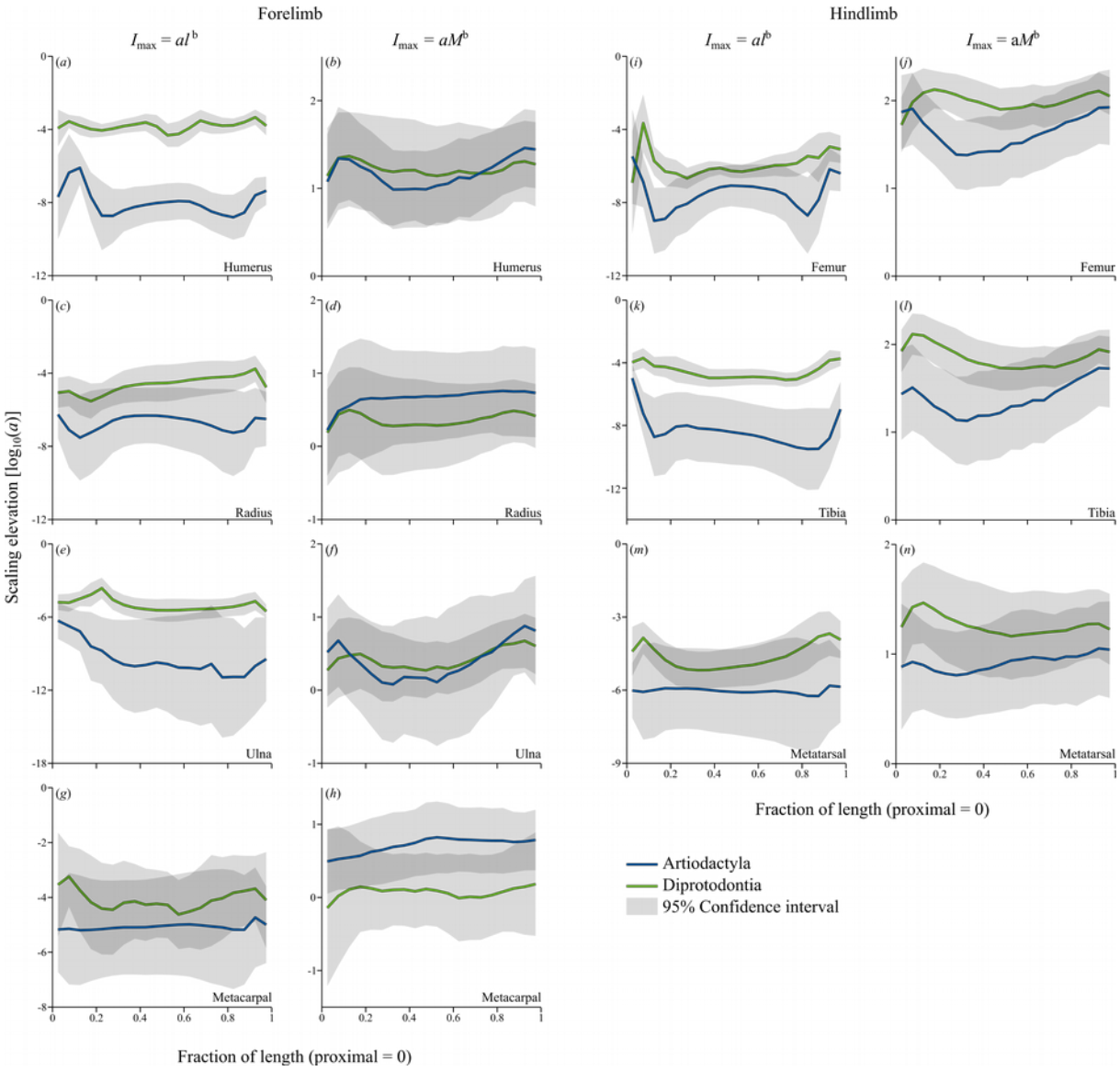

Figure 7. Scaling elevations [$\log_{10}(a)$] for second moment of area (I_{max}) versus bone length (l) and body mass (M) for all bones and both clades. Elevations are directly comparable only where slopes (scaling exponents, Figure 6) are equal. Light grey regions indicate the 95% confidence interval; dark grey regions occur where the confidence intervals overlap and may be interpreted as no significant difference in scaling elevation between clades.

References

1. Sun D, Brodt MD, Zannit HM, Holguin N, Silva MJ. 2017 Evaluation of loading parameters for murine axial tibial loading: Stimulating cortical bone formation while reducing loading duration. *J. Orthop. Res. Off. Publ. Orthop. Res. Soc.* (doi:10.1002/jor.23727)

2. Meakin LB, Price JS, Lanyon LE. 2014 The Contribution of Experimental in vivo Models to Understanding the Mechanisms of Adaptation to Mechanical Loading in Bone. *Front. Endocrinol.* **5**. (doi:10.3389/fendo.2014.00154)

3. Jacobs JM, Cameron KL, Bojescul JA. 2014 Lower extremity stress fractures in the military. *Clin. Sports Med.* **33**, 591–613. (doi:10.1016/j.csm.2014.06.002)

4. Boudrieau RJ, Dee JF, Dee LG. 1984 Central tarsal bone fractures in the racing Greyhound: a review of 114 cases. *J. Am. Vet. Med. Assoc.* **184**, 1486–1491.

5. O'Sullivan CB, Lumsden JM. 2003 Stress fractures of the tibia and humerus in Thoroughbred racehorses: 99 cases (1992-2000). *J. Am. Vet. Med. Assoc.* **222**, 491–8. (doi:12597423)

6. Verheyen KLP, Newton JR, Price JS, Wood JLN. 2006 A case-control study of factors associated with pelvic and tibial stress fractures in Thoroughbred racehorses in training in the UK. *Prev. Vet. Med.* **74**, 21–35. (doi:S0167-5877(06)00016-X)

7. Campione NE, Evans DC. 2012 A universal scaling relationship between body mass and proximal limb bone dimensions in quadrupedal terrestrial tetrapods. *BMC Biol.* **10**, 60. (doi:10.1186/1741-7007-10-60)

8. Alexander RM, Vernon A. 1975 The mechanics of hopping by kangaroos (Macropodidae). *J. Zool.* **177**, 265–303. (doi:10.1111/j.1469-7998.1975.tb05983.x)

9. Windsor DE, Dagg AI. 1971 The gaits of the Macropodinae (Marsupialia). *J. Zool.* **163**, 165–175. (doi:10.1111/j.1469-7998.1971.tb04530.x)

10. Clancy TF, Croft DB. 1991 Differences in Habitat Use and Grouping Behavior between Macropods and Eutherian Herbivores. *J. Mammal.* **72**, 441–449. (doi:10.2307/1382126)

11. O'Connor SM, Dawson TJ, Kram R, Donelan JM. 2014 The kangaroo's tail propels and powers pentapedal locomotion. *Biol. Lett.* **10**, 20140381. (doi:10.1098/rsbl.2014.0381)

12. Caughley G. 1964 Social Organization and Daily Activity of the Red Kangaroo and the Grey Kangaroo. *J. Mammal.* **45**, 429–436. (doi:10.2307/1377416)

13. Snelling EP, Biewener AA, Hu Q, Taggart DA, Fuller A, Mitchell D, Maloney SK, Seymour RS. 2017 Scaling of the ankle extensor muscle-tendon units and the biomechanical implications for bipedal hopping locomotion in the post-pouch kangaroo *Macropus fuliginosus*. *J. Anat.* (doi:10.1111/joa.12715)

14. Wells RT, Tedford RH. 1995 *Sthenurus* (Macropodidae, Marsupialia) from the Pleistocene

of Lake Callabonna, South Australia. *Bull. Am. Mus. Nat. Hist.* **225**.

15. Janis CM, Buttrill K, Figueirido B. 2014 Locomotion in Extinct Giant Kangaroos: Were Sthenurines Hop-Less Monsters? *PLOS ONE* **9**, e109888. (doi:10.1371/journal.pone.0109888)

16. Bennett MB, Taylor GC. 1995 Scaling of elastic strain energy in kangaroos and the benefits of being big. *Nature* **378**, 56–59. (doi:10.1038/378056a0)

17. Amson E, Kolb C. 2016 Scaling effect on the mid-diaphysis properties of long bones—the case of the Cervidae (deer). *Sci. Nat.* **103**, 58. (doi:10.1007/s00114-016-1379-7)

18. Biancardi CM, Minetti AE. 2012 Biomechanical determinants of transverse and rotary gallop in cursorial mammals. *J. Exp. Biol.* **215**, 4144–4156. (doi:10.1242/jeb.073031)

19. Basu C. 2018 The evolution of locomotor form and function in the giraffe lineage. PhD Thesis, The Royal Veterinary College, University of London, London, UK.

20. Hildebrand M. 1980 The Adaptive Significance of Tetrapod Gait Selection. *Integr. Comp. Biol.* **20**, 255–267. (doi:10.1093/icb/20.1.255)

21. Munn AJ, Dawson TJ, McLeod SR. 2010 Feeding biology of two functionally different foregut-fermenting mammals, the marsupial red kangaroo and the ruminant sheep: how physiological ecology can inform land management. *J. Zool.* **282**, 226–237. (doi:10.1111/j.1469-7998.2010.00740.x)

22. Prideaux GJ, Ayliffe LK, DeSantis LRG, Schubert BW, Murray PF, Gagan MK, Cerling TE. 2009 Extinction implications of a chenopod browse diet for a giant Pleistocene kangaroo. *Proc. Natl. Acad. Sci.* **106**, 11646–11650. (doi:10.1073/pnas.0900956106)

23. Alexander RM. 1977 Allometry of the limbs of antelopes (Bovidae). *J. Zool.* **183**, 125–146. (doi:10.1111/j.1469-7998.1977.tb04177.x)

24. Biewener AA. 1983 Allometry of quadrupedal locomotion: the scaling of duty factor, bone curvature and limb orientation to body size. *J. Exp. Biol.* **105**, 147–171.

25. McMahon TA. 1975 Allometry and Biomechanics: Limb Bones in Adult Ungulates. *Am. Nat.* **109**, 547–563. (doi:10.1086/283026)

26. Alexander R, Jayes A, Maloiy G, Wathuta E. 1979 Allometry of the limb bones of mammals from shrews (*Sorex*) to elephant (*Loxodonta*). *J. Zool.* **189**, 305–314. (doi:10.1111/j.1469-7998.1979.tb03964.x)

27. Bennett MB. 2000 Unifying principles in terrestrial locomotion: do hopping Australian marsupials fit in? *Physiol. Biochem. Zool. PBZ* **73**, 726–735. (doi:10.1086/318110)

28. McGowan CP, Skinner J, Biewener AA. 2008 Hind limb scaling of kangaroos and wallabies (superfamily Macropodoidea): implications for hopping performance, safety factor and elastic savings. *J. Anat.* **212**, 153–163. (doi:10.1111/j.1469-7580.2007.00841.x)

29. Kram R, Dawson TJ. 1998 Energetics and biomechanics of locomotion by red kangaroos (*Macropus rufus*). *Comp. Biochem. Physiol. B Biochem. Mol. Biol.* **120**, 41–49.

30. Doube M, Wiktorowicz-Conroy AM, Christiansen P, Hutchinson JR, Shefelbine S. 2009 Three-dimensional geometric analysis of felid limb bone allometry. *PLoS ONE* **4**, e4742. (doi:10.1371/journal.pone.0004742)

31. Doube M, Yen SCW, Kłosowski MM, Farke AA, Hutchinson JR, Shefelbine SJ. 2012 Whole-bone scaling of the avian pelvic limb. *J. Anat.* **221**, 21–29. (doi:10.1111/j.1469-7580.2012.01514.x)

32. Doube M, Kłosowski MM, Arganda-Carreras I, Cordelières F, Dougherty RP, Jackson J, Schmid B, Hutchinson JR, Shefelbine SJ. 2010 BoneJ: free and extensible bone image analysis in ImageJ. *Bone* **47**, 1076–1079. (doi:10.1016/j.bone.2010.08.023)

33. Doube M. 2016 bonej-org/bonej: BoneJ version 1.4.2. *Zenodo* (doi:10.5281/zenodo.154376)

34. Rasband WS. 2009 *ImageJ*. Bethesda, Maryland, USA: U.S. National Institutes of Health. See http://rsb.info.nih.gov/ij/.

35. Doube M, Felder AA. 2017 Scripts, queries, and database tables to accompany Doube et al. 2018. *figshare* (doi:10.6084/m9.figshare.5631994)

36. Silva M. 1995 *CRC Handbook of Mammalian Body Masses*. Boca Raton: CRC Press.

37. Helgen KM, Wells RT, Kear BP, Gerdtz WR, Flannery TF. 2006 Ecological and evolutionary significance of sizes of giant extinct kangaroos. *Aust. J. Zool.* **54**, 293–303. (doi:10.1071/ZO05077)

38. Jones KE *et al.* 2009 PanTHERIA: a species-level database of life history, ecology, and geography of extant and recently extinct mammals. *Ecology* **90**, 2648–2648. (doi:10.1890/08-1494.1)

39. Ferreira JL, Lopes FB, Bresolin T, Garcia JAS, Minharro S, Lôbo RB. 2015 Effect of age of dam on weight of calf in the genetic assessment of Zebu cattle in random regression models. *Acta Sci. Anim. Sci.* **37**, 203. (doi:10.4025/actascianimsci.v37i2.25355)

40. Spence AJ. 2009 Scaling in biology. *Curr. Biol. CB* **19**, R57-61. (doi:10.1016/j.cub.2008.10.042)

41. Warton DI, Duursma RA, Falster DS, Taskinen S. 2012 smatr 3– an R package for estimation and inference about allometric lines. *Methods Ecol. Evol.* **3**, 257–259. (doi:10.1111/j.2041-210X.2011.00153.x)

42. R Core Team. 2013 *R: A Language and Environment for Statistical Computing*. Vienna, Austria: R Foundation for Statistical Computing. See http://www.R-project.org.

43. Warton DI, Wright IJ, Falster DS, Westoby M. 2006 Bivariate line-fitting methods for allometry. *Biol. Rev.* **81**, 259–291. (doi:10.1017/S1464793106007007)

44. Felsenstein J. 1985 Phylogenies and the comparative method. *Am. Nat.* **125**, 1–15.

45. Bininda-Emonds ORP *et al.* 2007 The delayed rise of present-day mammals. *Nature* **446**, 507–512. (doi:10.1038/nature05634)

46. Garcia GJM, da Silva JKL. 2006 Interspecific allometry of bone dimensions: A review of the theoretical models. *Phys. Life Rev.* **3**, 188–209. (doi:10.1016/j.plrev.2006.07.002)

47. Sorkin B. 2008 Limb bone stresses during fast locomotion in the African lion and its bovid prey. *J. Zool.* **276**, 213–218. (doi:10.1111/j.1469-7998.2008.00477.x)

48. Blob RW, Espinoza NR, Butcher MT, Lee AH, D'Amico AR, Baig F, Sheffield KM. 2014 Diversity of Limb-Bone Safety Factors for Locomotion in Terrestrial Vertebrates: Evolution and Mixed Chains. *Integr. Comp. Biol.* , icu032. (doi:10.1093/icb/icu032)

49. Skedros JG, Dayton MR, Sybrowsky CL, Bloebaum RD, Bachus KN. 2003 Are uniform regional safety factors an objective of adaptive modeling/remodeling in cortical bone? *J. Exp. Biol.* **206**, 2431–2439. (doi:10.1242/jeb.00466)

50. Carlson KJ, Judex S. 2007 Increased non-linear locomotion alters diaphyseal bone shape. *J. Exp. Biol.* **210**, 3117–3125. (doi:10.1242/jeb.006544)

51. Weatherholt AM, Warden SJ. 2018 Throwing enhances humeral shaft cortical bone properties in pre-pubertal baseball players: a 12-month longitudinal pilot study. *J. Musculoskelet. Neuronal Interact.* **Accepted**.

52. De Souza RL, Matsuura M, Eckstein F, Rawlinson SCF, Lanyon LE, Pitsillides AA. 2005 Non-invasive axial loading of mouse tibiae increases cortical bone formation and modifies trabecular organization: a new model to study cortical and cancellous compartments in a single loaded element. *Bone* **37**, 810–818. (doi:10.1016/j.bone.2005.07.022)

53. Weatherholt AM, Fuchs RK, Warden SJ. 2013 Cortical and trabecular bone adaptation to incremental load magnitudes using the mouse tibial axial compression loading model. *Bone* **52**, 372–379. (doi:10.1016/j.bone.2012.10.026)

54. Berman AG, Clauser CA, Wunderlin C, Hammond MA, Wallace JM. 2015 Structural and Mechanical Improvements to Bone Are Strain Dependent with Axial Compression of the Tibia in Female C57BL/6 Mice. *PloS One* **10**, e0130504. (doi:10.1371/journal.pone.0130504)

55. DeSouza R, Javaheri B, Collinson RS, Chenu C, Shefelbine SJ, Lee PD, Pitsillides AA. 2017 Prolonging disuse in aged mice amplifies cortical but not trabecular bones' response to mechanical loading. *J. Musculoskelet. Neuronal Interact.* **17**, 218–225.

56. Meakin LB, Delisser PJ, Galea GL, Lanyon LE, Price JS. 2015 Disuse rescues the age-impaired adaptive response to external loading in mice. *Osteoporos. Int. J. Establ. Result Coop. Eur. Found. Osteoporos. Natl. Osteoporos. Found. USA* **26**, 2703–2708. (doi:10.1007/s00198-015-3142-x)

57. Firth EC, Rogers CW, van Weeren PR, Barneveld A, McIlwraith CW, Kawcak CE, Goodship AE, Smith RKW. 2011 Mild exercise early in life produces changes in bone size and strength but not density in proximal phalangeal, third metacarpal and third carpal bones of foals. *Vet. J.* **190**, 383–389. (doi:10.1016/j.tvjl.2010.11.016)

58. Firth EC, Rogers CW, Doube M, Jopson NB. 2005 Musculoskeletal responses of 2-year-old Thoroughbred horses to early training. 6. Bone parameters in the third metacarpal and third metatarsal bones. *N. Z. Vet. J.* **53**, 101–112. (doi:10.1080/00480169.2005.36487)

59. Blumstein DT, Evans CS, Daniel JC. 1999 An experimental study of behavioural group size effects in tammar wallabies, *Macropus eugenii*. *Anim. Behav.* **58**, 351–360. (doi:10.1006/anbe.1999.1156)

60. Ord TJ, Cooper DW, Evans CS. 1999 Nocturnal behaviour of the parma wallaby, *Macropus parma* (Marsupialia : Macropodoidea). *Aust. J. Zool.* **47**, 155. (doi:10.1071/ZO98047)

61. Blumstein DT, Daniel JC, Sims RA. 2003 Group size but not distance to cover influences agile wallaby (*Macropus agilis*) time allocation. *J. Mammal.* **84**, 197–204.

62. Grant TR. 1974 Observation of enclosed and free-ranging grey kangaroos *Macropus giganteus*. *Z. Für Säugetierkd.* **39**, 65–78.

63. Martin J, Benhamou S, Yoganand K, Owen-Smith N. 2015 Coping with spatial heterogeneity and temporal variability in resources and risks: adaptive movement behaviour by a large grazing herbivore. *PloS One* **10**, e0118461. (doi:10.1371/journal.pone.0118461)

64. Ensing EP, Ciuti S, de Wijs FALM, Lentferink DH, Ten Hoedt A, Boyce MS, Hut RA. 2014 GPS based daily activity patterns in European red deer and North American elk (Cervus elaphus): indication for a weak circadian clock in ungulates. *PloS One* **9**, e106997. (doi:10.1371/journal.pone.0106997)

65. Leuthold BM, Leuthold W. 1978 Daytime activity patterns of gerenuk and giraffe in Tsavo National Park, Kenya. *Afr. J. Ecol.* **16**, 231–243. (doi:10.1111/j.1365-2028.1978.tb00444.x)

66. Seeber PA, Ciofolo I, Ganswindt A. 2012 Behavioural inventory of the giraffe (Giraffa camelopardalis). *BMC Res. Notes* **5**, 650. (doi:10.1186/1756-0500-5-650)

67. Perry AK, Blickhan R, Biewener AA, Heglund NC, Taylor CR. 1988 Preferred speeds in terrestrial vertebrates: are they equivalent? *J. Exp. Biol.* **137**, 207–219.

68. Arnold AS, Lee DV, Biewener AA. 2013 Modulation of joint moments and work in the goat hindlimb with locomotor speed and surface grade. *J. Exp. Biol.* **216**, 2201–2212. (doi:10.1242/jeb.082495)

69. Biewener AA, Taylor CR. 1986 Bone strain: a determinant of gait and speed? *J. Exp. Biol.* **123**, 383–400.

70. Conte S, Bergeron R, Gonyou H, Brown J, Rioja-Lang FC, Connor L, Devillers N. 2014 Measure and characterization of lameness in gestating sows using force plate, kinematic, and accelerometer methods. *J. Anim. Sci.* **92**, 5693–5703. (doi:10.2527/jas.2014-7865)

71. Pike AVL, Alexander RM. 2002 The relationship between limb-segment proportions and joint kinematics for the hind limbs of quadrupedal mammals. *J. Zool.* **258**, 427–433. (doi:10.1017/S0952836902001577)

72. McGowan CP, Baudinette RV, Usherwood JR, Biewener AA. 2005 The mechanics of jumping versus steady hopping in yellow-footed rock wallabies. *J. Exp. Biol.* **208**, 2741–2751. (doi:10.1242/jeb.01702)

73. McGowan CP, Baudinette RV, Biewener AA. 2008 Differential design for hopping in two species of wallabies. *Comp. Biochem. Physiol. A. Mol. Integr. Physiol.* **150**, 151–158. (doi:10.1016/j.cbpa.2006.06.018)

74. Farley CT, Glasheen J, McMahon TA. 1993 Running springs: speed and animal size. *J. Exp. Biol.* **185**, 71–86.

75. Lanyon LE, Bourn S. 1979 The influence of mechanical function on the development and remodeling of the tibia. An experimental study in sheep. *J. Bone Joint Surg. Am.* **61**, 263–273. (doi:10.2106/00004623-197961020-00019)

76. Felder AA, Phillips C, Cornish H, Cooke M, Hutchinson JR, Doube M. 2017 Secondary osteons scale allometrically in mammalian humerus and femur. *R. Soc. Open Sci.* **4**, 170431. (doi:10.1098/rsos.170431)

77. Doube M, Kłosowski MM, Wiktorowicz-Conroy AM, Hutchinson JR, Shefelbine SJ. 2011 Trabecular bone scales allometrically in mammals and birds. *Proc. R. Soc. B* **278**, 3067–3073. (doi:10.1098/rspb.2011.0069)

78. Doube M, Kłosowski MM, Hutchinson JR, Shefelbine SJ. 2017 CT and XMT image data of diprotodont and artiodactyl limb bones to accompany Doube et al. 2018. *figshare* (doi:10.6084/m9.figshare.5634208)

Source	Accession number	Order	Binomial	Familiar name	*M* (kg)	Bone length (mm)						
						humerus	radius	ulna	mc	femur	tibia	mt
UMZC	H15052	Artiodactyla	*Tragulus kanchil*	lesser mouse-deer	1.62	68.7	57.0	67.7	39.3	78.3	91.0	58.4
UMZC	H14975	Artiodactyla	*Tragulus napu*	greater mouse-deer	5.27	84.7	-	-	49.8	101.1	117.1	70.6
UMZC	H.15532	Artiodactyla	*Muntiacus reevesi*	Reeves' muntjac	13.50	93.3	80.2	99.3	59.6	114.7	123.4	83.9
NHM	ZD 1863.12.29.1	Artiodactyla	*Cephalophus dorsalis*	Bay duiker	20.00	124.2	106.9	132.3	85.8	152.8	151.7	97.8
NHM	ZD 1974.414	Artiodactyla	*Antilope cervicapra*	blackbuck	36.30	151.4	171.9	207.0	185.4	185.7	227.8	192.6
RVC	alpaca1	Artiodactyla	*Vicugna vicugna*	alpaca	45.00	-	-	-	-	265.8	-	-
RVC	goat1	Artiodactyla	*Capra hircus*	goat	48.00	-	-	-	-	216.5	-	-
RVC	sheep2	Artiodactyla	*Ovis aries*	domestic sheep	57.00	-	-	-	-	192.8	-	-
NHM	ZD 1961.8.9.80	Artiodactyla	*Cephalophus sylvicultor*	yellow-backed duiker	61.30	193.2	176.7	219.6	155.4	232.3	242.6	170.2
UMZC	H.16232	Artiodactyla	*Cervus davidianus*	Pere David's deer	182.00	255.2	261.5	314.0	244.6	327.8	339.4	263.9
NHM	ZD 1963.10.21.1	Artiodactyla	*Oryx beisa*	beisa	200.58	243.2	273.2	336.5	224.1	309.4	322.6	232.9
UMZC	H.20302	Artiodactyla	*Okapia johnstoni*	okapi	230.00	317.5	350.2	418.0	309.4	328.4	353.1	324.7
UMZC	H.16634	Artiodactyla	*Cervus elaphus*	red deer	240.87	-	266.9	314.2	231.6	278.0	329.0	265.1
NHM	47	Artiodactyla	*Bos indicus*	zebu	275.00	178.3	190.5	229.1	-	221.8	228.8	-
UMZC	H.17691	Artiodactyla	*Alces alces*	Eurasian elk	461.90	387.8	401.1	491.5	343.0	445.9	492.7	406.4
RVC	WindfallLgGiraffe	Artiodactyla	*Giraffa camelopardalis*	giraffe	482.00	410.3	628.0	416.3	587.7	457.9	525.8	580.5
RVC	cow2	Artiodactyla	*Bos taurus*	cattle	500.00	-	-	-	-	415.9	-	-
UMZC	H.17535	Artiodactyla	*Megaloceros giganteus*	Irish elk	585.00	405.1	402.1	501.3	334.9	-	477.6	370.5
NHM	ZD 1874.11.2.4	Artiodactyla	*Syncerus caffer*	African buffalo	592.67	347.8	316.9	404.0	187.3	411.0	387.5	216.0
UMZC	H.10707-H.10715	Artiodactyla	*Hippopotamus amphibius*	hippopotamus	1536.31	453.7	276.4	384.9	-	474.4	339.0	-
NHM	ZD 1851.4.24.2	Diprotodontia	*Potorous tridactylus*	long-nosed potoroo	1.05	39.3	45.1	55.6	12.0	75.2	83.4	30.3
NHM	ZD 1858.5.26.23	Diprotodontia	*Bettongia penicillata*	woylie	1.18	33.6	44.1	52.7	10.1	80.1	104.4	44.4
NHM	ZD 277.p	Diprotodontia	*Bettongia lesueur*	boodie	1.45	22.8	28.5	35.6	6.9	56.8	75.6	38.9
UMZC	A12.79/1	Diprotodontia	*Bettongia gaimardi*	Eastern bettong	1.67	33.3	38.2	47.6	-	84.4	99.5	46.4
NHM	ZD 1984.1002-1003	Diprotodontia	*Macropus parma*	Parma wallaby	4.16	70.1	85.2	98.4	14.1	134.2	168.5	57.9
UMZC	A12.59/2	Diprotodontia	*Onychogalea fraenata*	bridled nail-tail wallaby	4.95	71.9	79.4	92.6	-	119.5	185.0	56.3
NHM	ZD 1962.5.22.1	Diprotodontia	*Macropus eugenii*	Tammar wallaby	5.28	56.6	74.8	86.4	12.0	123.3	167.4	60.1
UMZC	A12.50/1	Diprotodontia	*Thylogale billardierii*	Tasmanian pademelon	5.87	78.3	91.5	107.5	-	134.7	165.1	52.1
UMZC	A12.52/2	Diprotodontia	*Petrogale xanthopus*	yellow-footed rock-wallaby	8.50	82.6	91.9	110.4	-	157.7	202.7	69.5
NHM	ZD 1970.2189	Diprotodontia	*Macropus agilis*	agile wallaby	11.82	85.3	108.4	126.0	20.5	169.8	239.4	94.5
NHM	ZD 1976.184	Diprotodontia	*Macropus rufogriseus*	Bennett's wallaby	16.85	126.2	138.4	157.2	19.4	199.3	285.1	98.6

NHM	ZD 1961.12.11.1	Diprotodontia	*Macropus fuliginosus*	Western grey kangaroo	25.56	82.3	109.0	128.0	17.3	189.3	290.4	101.4
UMZC	A12.19/1	Diprotodontia	*Macropus robustus*	wallaroo	25.98	97.8	135.7	159.5	-	207.5	326.4	113.8
UMZC	A12.17/1	Diprotodontia	*Macropus giganteus*	Eastern grey kangaroo	60.00	175.1	235.0	266.4	-	267.5	473.9	166.3
UMZC	A12.17/4	Diprotodontia	*Macropus giganteus*	Eastern grey kangaroo	60.00	216.5	280.2	326.6	-	299.7	543.2	183.8
NHM	ZD 2010.8	Diprotodontia	*Macropus rufus*	red kangaroo	72.50	212.3	310.8	348.2	36.2	300.5	572.7	179.6

470 **Table 1. List of specimens**. Complete list of specimens, their body masses and lengths of bones used for scaling calculations. Some bones from some specimens were not available to study and are indicated as a dash. NHM, Natural History Museum (London); UMZC, University Museum of Zoology, Cambridge; RVC, The Royal Veterinary College (authors' collections); mc, metacarpal; mt, metatarsal.

bone	Artiodactyl scaling exponent					Diprotodont scaling exponent					Equal slopes	Artiodactyl elevation			Diprotodont elevation			Equal elevations
	b	$-b$	$+b$	R^2	p	b	$-b$	$+b$	R^2	p	p_b	$\log_{10}(a)$	$-\log_{10}(a)$	$+\log_{10}(a)$	$\log_{10}(a)$	$-\log_{10}(a)$	$+\log_{10}(a)$	p_a
humerus	0.317	0.270	0.372	0.928	< 0.001	0.463	0.384	0.558	0.892	< 0.001	0.003							
radius	0.357	0.275	0.464	0.804	< 0.001	0.487	0.416	0.571	0.923	< 0.001	0.042							
ulna	0.333	0.272	0.408	0.884	< 0.001	0.468	0.401	0.547	0.927	< 0.001	0.009							
metacarpal	0.425	0.337	0.535	0.863	< 0.001	0.323	0.219	0.477	0.800	< 0.001	0.198	1.470	1.298	1.642	0.858	0.739	0.977	< 0.001
femur	0.299	0.258	0.346	0.917	< 0.001	0.353	0.311	0.400	0.951	< 0.001	0.788	1.735	1.661	1.810	1.858	1.817	1.899	< 0.001
tibia	0.282	0.227	0.350	0.857	< 0.001	0.447	0.408	0.491	0.974	< 0.001	< 0.001							
metatarsal	0.369	0.294	0.462	0.870	< 0.001	0.392	0.349	0.442	0.957	< 0.001	0.608	1.545	1.440	1.651	1.519	1.472	1.566	0.500

Table 2. Summary statistics for bone length scaling against body mass, where $l = aM^b$. The scaling exponent (slope, b) is indicated alongside its upper and lower 95% confidence limits ($\pm b$), along with the coefficient of determination (R^2) and p indicating the strength of the correlation between bone length and body mass values. The likelihood of equality of scaling exponents between artiodactyl and diprotodont bones is indicated by p_b. Where slopes are not significantly different, elevations ($\log_{10}(a)$), their 95% confidence limits ($\pm\log_{10}(a)$), and equality of elevations between artiodactyls and diprotodonts (p_a) are reported. Statistical estimates were generated by R calls using smatr on data in Table 1., 'animal_table', e.g.:

```
> summary(sma(log10(animal_table$humerus)~log10(mass)*order))
> summary(sma(log10(animal_table$humerus)~log10(mass)+order, type="elevation"))
```

bone	Artiodactyl PIC scaling exponent					Diprotodont PIC scaling exponent				
	b	*-b*	*+b*	R^2	*p*	*b*	*-b*	*+b*	R^2	*p*
					$l \propto M^b$					
humerus	0.354	0.298	0.420	0.917	< 0.001	0.550	0.396	0.762	0.719	< 0.001
radius	0.401	0.320	0.503	0.855	< 0.001	0.555	0.418	0.739	0.767	< 0.001
ulna	0.376	0.306	0.462	0.881	< 0.001	0.538	0.407	0.710	0.779	< 0.001
metacarpal	0.449	0.341	0.590	0.806	< 0.001	0.368	0.221	0.612	0.646	< 0.001
femur	0.420	0.323	0.545	0.734	< 0.001	0.362	0.285	0.461	0.836	< 0.001
tibia	0.330	0.266	0.409	0.858	< 0.001	0.472	0.386	0.576	0.898	< 0.001
metatarsal	0.401	0.309	0.520	0.824	< 0.001	0.450	0.382	0.530	0.925	< 0.001
					$I_{max} \propto M^b$					
humerus	1.808	1.579	2.070	0.949	< 0.001	2.033	1.364	3.031	0.575	0.0016
radius	1.810	1.493	2.193	0.896	< 0.001	1.966	1.328	2.911	0.548	0.0016
ulna	1.793	1.505	2.136	0.914	< 0.001	1.955	1.372	2.786	0.636	< 0.001
metacarpal	1.828	1.549	2.158	0.930	< 0.001	1.504	1.048	2.160	0.829	< 0.001
femur	2.001	1.526	2.626	0.712	< 0.001	1.592	1.272	1.992	0.858	< 0.001
tibia	1.706	1.391	2.092	0.871	< 0.001	1.574	1.234	2.007	0.848	< 0.001
metatarsal	1.784	1.490	2.136	0.917	< 0.001	1.699	1.384	2.087	0.881	< 0.001

Table 3 Bone length and mid-shaft second moment of area phylogenetically independent contrasts scaling exponents against body mass, where $l \propto M^b$ or $I_{max} \propto M^b$. The scaling exponent (slope, *b*) is indicated alongside its upper and lower 95% confidence limits (±*b*), along with the coefficient of determination (R^2) and *p* indicating the strength of the correlation between bone length and body mass values.